Modelling of Plasma Loudspeakers

Ph. BÉQUIN* and K. CASTOR

Laboratoire d'Acoustique de l'Université du Maine - UMR CNRS 6613 F72085 - Le Mans cedex 9 (France).

Ph. HERZOG

Laboratoire de Mécanique et d'Acoustique - UPR 7051 F13402 - Marseille cedex 20 (France).

V. MONTEMBAULT

Laboratoire d'Acoustique de l'Université du Maine - UMR CNRS 6613 F72085 - Le Mans cedex 9.

(Dated: 8 février 2006)

This paper is based on the acoustic modelling and measurements of a needle-to-grid plasma loudspeaker using a negative Corona discharge.

The first part summarises the model described in previous papers, where the electrode gap is divided into a charged particle production region near the needle and a drift region which occupies most of the inter-electrodes gap. In each region, interactions between charged and neutral particles in the ionised gas lead to a perturbation of surrounding air, and so generate an acoustic field. For each region, seen as a separate acoustic source, an acoustical model requiring a few parameters is proposed.

The second part of the paper presents an experimental set-up for measuring acoustic pressure and directivities, which has been developed and used to study the evolutions of the parameters with physical properties such as geometric and electric configuration, or the needle material.

The final part of this paper is devoted to a study of the electroacoustic efficiency of the plasma loudspeaker, and the analysis of its variations with the design parameters. This work thus aims to providing the first data required for an optimisation.

PACS numbers: 43.38.+n,44.15.+a,52.35.Fb,43.28.Ra,51.50.+v

I. INTRODUCTION

In plasma loudspeaker, the ionised gas from discharges is used to convert electrical signals into acoustic perturbations. The development of this kind of loudspeaker arose from a need by audiophile to achieve a transducer with no moving parts, yielding a wide frequency range. A very good description of the historical background, the basic principles and the application of gas discharges to loudspeakers are given in references 1, 2. A first description of the physics involved in audio devices was published in 1982 by Bondar[3,4] and a description of some devices can be found in references 5. Moreover, many publications deal with the physics of energy transfer inside ionised gases (*e.g.* refs. 6–10), including the phenomena we are considering. Last, a strong background about electric discharges in gases can be found in references 11–14.

Plasma loudspeakers reported in the literature are divided into two classes with significant different gross physical properties : so-called "hot-plasma" and "cold-plasma" loudspeakers, in which the preponderant acoustic source is respectively a heat or a force source, and having respectively a monopolar or dipolar behaviour[3,4]. For the major part of the plasma loudspeakers developed until now, an ionised gas is obtained by application of high voltage (D.C. or A.C.) between electrodes having different curvature radii (e.g. a point and a plane). The complex phenomena which take place in the electrode gap are called discharges in the gas. These discharges present different physical behaviours or regimes depending on the polarity of the small-radius electrode, the point radius, the gap length and the gas[1,11,15–18].

By choosing the appropriate geometric and electric configurations of the electrodes, but also depending on the location relative to the electrodes, the interactions between charged and neutral particles in the ionised gas can lead to either a predominant heat transfer (Joule heat source, almost isotropic) or a predominant momentum transfer which creates a gas flow, the so-called "electric wind" (force source, having a specific

*Electronic address: Philippe.Bequin@univ-lemans.fr

axis). Time variation of the heating of an air volume produces a corresponding pressure change. The "hot-plasma" loudspeakers using this principle are mainly flame sources[19–21], the thermophone used for calibrating microphones[22], the glow discharges[2,23], the spark discharges[24,25], and the ionophone[26–28]. By contrast, "cold plasma" loudspeakers are based on momentum transfer, which has been described for the first time in 1972 by Matsuzawa[29] : a negative voltage is applied to the points of a multipoints-grid electrode system, generating a corona discharge in air. Negative ions are attracted by the positive electrode (grid), and thus tend to drift along the electrical field lines. This is the source of the "electric wind", which is modulated by combining an audio-frequency alternating component with the DC one.

The present work therefore starts from the phenomena involved in negative discharges, to understand how these interact to give rise to the two source mechanisms (heat and force source) already mentioned. Because these are highly correlated, we take them simultaneously into account, and point out that for usual situations they have the same order of magnitude. Some effects of varying the electrode shapes and discharge parameters are discussed, and demonstrated experimentally on sample prototypes. As this work is part of a more general and fundamental research program, it is limited to small sized laboratory experiments, but they seem to give useful trends which could be used for further investigations about actual laboratory or audio systems.

II. DESCRIPTION OF A CORONA LOUDSPEAKER

This section summarises the results presented in previous publications[30–33], focusing on the specific case of discharges in air at normal atmospheric conditions, obtained by applying a high negative voltage to a needle facing a grid (Figure 1).

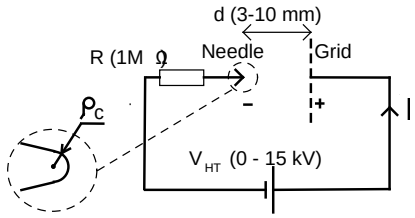

FIG. 1. Schematic diagram of a needle-to-grid discharges. V_{HT}, I, R, d and ρ_c represent respectively the supplied voltage, the electric current, the ballast resistance, the gap length and the curvature radius.

The gas between the two electrodes is assumed to be weakly ionised. The energy exchange between charged particles and neutral particles are complex and can take several forms. The charged particles in a weakly ionised gas acquire energy from the electric field and lose this energy through collisions with the neutral gas particles under randomised and organised form. The macroscopic description of the neutral gas inside the weakly ionised gas assumes that the collisions between neutral particles are dominant, and only the small disturbances generated by charged particles perturb the equilibrium of the system.

The interaction mechanisms between charged and neutral particles involve both collisional-momentum and thermal energy-exchange effects which are introduced in the equations of linear acoustics (the equations for mass, momentum and energy conservation) by two source terms[30–33] : a heat source H and a force source F. Assuming the gas of neutral particles as an ideal gas, adiabatic conditions, and a first-order expansion of the acoustic quantities, an Helmholtz equation can be obtained by use of the set of linearised acoustic equations (continuity, Euler and Fourier equations). This equation can be separated into a pair of uncoupled equations each one associated with one source. Finally, the sound pressure p_h and p_f , associated with the heat source and the force source respectively, may be obtained by calculating the integral solution of the Helmholtz equation, using the free-space Green function[30,32].

Such discharges have intrinsically both heat and momentum transfer, as can be understood from the above basic physics. A previous study by two of the authors[31] pointed out that both sources have a significant influence on the pressure radiation. They verified this experimentally on a simple negative polarity point-to-grid electrode system. The measured directivity curves are then close to a supercardioid pattern, showing the sum of a monopole, and a dipole with approximately twice the amplitude of the monopole[33]. This tendency is in accordance with a note from Tombs and Shirley[34,35] who pointed out a lack of symmetry in the radiation of their prototypes, although they did not give any explanation for this phenomenon.

A. Electrical behaviour

When a high voltage is applied to a small-radius electrode, air in the vicinity of the electrode becomes ionised. The charged particles so created form a cloud concentrating locally, and drifting along the field lines. The local presence of the cloud distorts the electric field which therefore varies with time as successive clouds drift from one electrode to the other. This phenomenon creates an electric current in the external circuit, in the form of successive so-called "Trichel's pulses" (see refs. 11, 15, 18, 36–39), which is characteristic of the

low-current behaviour.

The frequency of the pulses increases with the applied voltage, and progressively successive pulses overlap, leading to a DC current which also increases, and can even predominate when reaching the "pulseless" regime. Higher voltage can even lead to a spark. The geometric and electric configurations of the needle-to-grid system are adapted to provide a wide range of currents, although avoiding sparks. Figure 2 shows the non-linear relation between the current I and the applied voltage V_{HT}, showing a lower limit V_s for the voltage required to force current through the discharge. In the corona regime, an empirical relation between I and V_{HT} can be expressed as (see refs. 15, 16, 18, 36, 40) :

$$I = C\, V_{HT}(V_{HT} - V_S)$$

where C is a factor which depends on the gap length d and the ionic mobility.

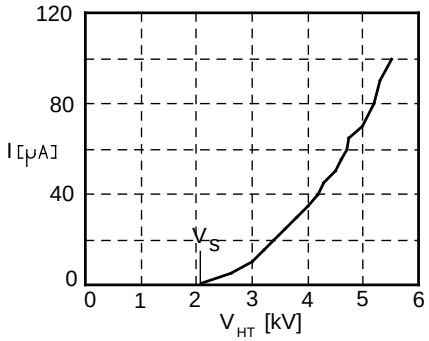

FIG. 2. Typical measured current-voltage ($I - V_{HT}$) characteristic of needle-to-grid air gap ($d = 3\ mm, \rho_c = 20\ \mu m$)

Considering a time-averaged repartition of the electric field in the gap, two regions can be distinguished (fig. 3) :

- the first one, termed the ionisation region, is located at the tip of the point and is characterised by a value of the field higher than the "critical" value of the electric field E_c for which electron production by ionisation is exactly compensated by attachment of the electrons on neutral particles ($E_c \simeq 27kV/cm$ in air) ;

- the second one, termed the drift region, takes place between the ionisation region and the plane, and is characterised by a weaker and an almost uniform value of the electric field[41].

As a consequence, considering an average over the Trichel's pulses period, it can be assumed that charged particles are created inside the ionisation region where their temperature is high, and that electrons and negative ions drift along the field lines through the drift region in which the collisions of charged particles with neutral particle induces movement of air known as electric wind or ionic wind (see refs. 42–48).

B. Electrical model

Kekez et al.[49] described the point-to-plane discharges in terms of an equivalent circuit which is composed of three elements (fig. 3) : a resistance r_i, taken inversely proportional to the electron density, which represents the ionisation region ; and a resistance r_u, taken inversely proportional to the negative ion density, shunted by a capacity C_u formed between the plane and ionisation region, which represents the drift region.

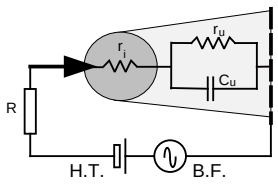

FIG. 3. Schematic representation of a needle-to-grid discharge. r_i, r_u and C_u denote the resistance of each region and the capacity of the drift region.

Measurements made by the authors[30–33,50] showed that this model seems to represent adequately the impedance of a single needle-to-grid system up to about $100kHz$, and that the sum of the values estimated for r_i and r_u by dynamic impedance measurements agree well with the static resistance estimated from the local slope of the $I - V_{HT}$ curve. The resistances r_u and r_i are estimated around $20\,M\Omega$ and $2\,M\Omega$ respectively. Their gross features are that both resistances decrease with increasing DC current I, and that they increase with increasing distance d at constant DC current. If the current flowing through the electrodes is modulated at acoustic frequencies by an external electronic circuit, the two energy transfer mechanisms act as two coupled acoustic sources, whereas the functioning regime is modulated around an operating point and travels along the $I - V_{HT}$ curve. It is thus expected that the transducer has a non-linear behaviour which cannot be avoided totally by using current drive, although it might be more adequate than voltage drive which exhibits an intrinsically quadratic behaviour.

C. Heat source model

In the ionisation region, the energy provided by the electric field to the charged particles is, in a large part, transferred to surrounding neutral particles as thermal energy. To establish an expression of the power per unit volume gained by the neutral particles, Bayle and others[7,8,10] have investigated the hydrodynamic equations of each particle type in a spherical volume and obtained the straightforward relation :

$$H = \mathcal{K}\mathbf{J}\mathbf{E} \tag{1}$$

where $\mathbf{J}$ denotes the total current density, $\mathbf{E}$ the total electric field in the ionisation region and the parameter $\mathcal{K}$ is the energy transfer rate between charged particles and surrounding neutral particles.

Considering the ionisation region as a small sphere (radius about $0.1\,mm$) centered on the point, with uniformity of the heat source inside this volume, we take into account only the total heat flux leaving the volume. The linearised part of H is then the power per unit volume dissipated by Joule effect, and can be expressed in function of the electric and the geometric model of the loudspeaker. Although the relation between the voltage, the current and the source terms are non-linear, only small current variations around an average value are considered[30,32], and the corresponding sound pressure p_h can be expressed as :

$$p_h(r,\omega) \approx j\omega\,\frac{\gamma-1}{c_o^2}\,\mathcal{K}[r_i I + (V_i - V_a)]\,\frac{e^{-jkr}}{4\pi r}\,i(\omega) \tag{2}$$

where $k = \omega/c_0$ (ω and c_0 are the pulsation and the adiabatic sound speed), and γ, V_a, V_i, I and i represent respectively the specific-heat ratio, the electric potentials at the point and at the interface between the two regions, the discharge current and the linearised current variation.

The amplitude of pressure is related to the electrical parameters of loudspeaker and shows a $+6\,dB/octave$ increase with frequency. Because the source is assumed isotropic and small enough, the pressure is described here as a pure monopole. In the above expression, only the quantity $\mathcal{K}(V_i - V_a)$ is unknown : it is a part of the total voltage applied to the electrodes, but the exact proportion cannot be determined theoretically without a suitable model for the electric field, which is beyond the scope of this paper. Consequently its value must be obtained from the experiments by adjusting the predicted acoustic levels.

D. Force source model

In the drift region, only the negative particles drift to the collecting grid along the electric field lines and exchange momentum with the neutral particles during collisions. The electrons are considerably lighter than negative ions, and consequently it is assumed that the electrons action on the neutral particles is negligible compared to the negative ions action. Furthermore, the heating of the neutral particle gas is considered as negligible. Assuming the mass ratio between negative ion and neutral particle close to unity, the vector force $\mathbf{F}$ per unit volume applied to the neutral particles can be written as[30,32] :

$$\mathbf{F} = N_i\,q_i\,\mathbf{E} \tag{3}$$

where the quantities N_i, q_i ,$\mathbf{E}$ represent respectively the negative ion density, their charge and the vector electric field inside the drift region.

Geometrical reasons lead to the adoption of a cylindrical coordinate system. The drift region is represented by a cylinder (with radius ρ_d and length d) in which the electric field is assumed to be uniform along and around the axis of the point. Considering the case where all dimensions of the drift region are small compared to the wavelength λ, the sound pressure in far field can be expressed as[32] :

$$p_f(r,\omega) \approx \frac{1}{\mu_i(\beta+1)}\,\frac{i(\omega)}{(1+j\omega r_u C_u)}\,\frac{(1+jkr)d\cos\theta}{r}\,\frac{e^{-jkr}}{4\pi r} \tag{4}$$

where θ, $\beta = I_e/I_i$, μ_i and i, are respectively the observation angle, the ratio of electric currents I_e and I_i carried by the electrons and the ions, the mobility of negative ion ($\approx 1.8\ 10^{-4} V.m^2/s$), and the linearised current variation.

The pressure expression (4) predicts a null slope at very low frequencies (proximity effect), then a $+6\,dB/octave$ slope until a first-order pole related to the electric impedance of the drift region, as shown by the denominator term $(1 + j\omega r_u C_u)$. Its directivity pattern is dipolar with the above assumption, but at higher frequencies (above $10kHz$ for usual configurations) interferences occur throughout the gap, leading to a higher-order directivity pattern, and a sharp cut-off when $kd \approx \pi/2$. As in the heat source model, there is an unknown quantity, the ratio $\beta = I_e/I_i$, for which only an order of magnitude may be found in publications about electric discharges. Its actual value will therefore also be deduced from the experimental results.

E. Total pressure

The total pressure p_t is the sum of the pressure p_h (Eq. 2) which is expressed assuming a pole located at the tip of the point, and the pressure p_f (Eq. 4) with a dipole centered in the gap. The analytical convenience of these incompatible choices is to maintain for each source the symmetry of the related problem, and consequently to analyse more easily their respective directivity. In practice, during directivity measurements, the origin of the needle-to-grid system is more or less centred on the gap. Thus the distance between the heat source and the microphone is varying, depending on the observation angle. However this angle dependence of the observation distance can reasonably be assumed negligible in the far field, at least for frequencies low enough so that the corresponding phase lag is unimportant.

Keeping in mind the above remarks, the total pressure p_t can be modelled as the sum of the analytical expression of p_h and p_f, showing a frequency response having a $+6\,dB/octave$ slope in most of the audio spectrum, and a general cardioïd directivity pattern resulting of the sum of a monopole pressure p_h and a dipole pressure p_f. At lower frequencies (or closer to the source) the near-field term of the dipole predominates, and at very high frequencies the monopole behaviour takes over as the gap resistance is shunted by its capacitance.

Because both terms are described by a volume integral, with integrands including source terms, this analytical model can be extended to the case of multiple points. Assuming they all have a similar electrical behaviour, a simple convolution of the Green function can be done over the spatial repartition of the points. For small enough transducers, and in far field, this sum may lead to an equivalent transducer combining the strength of all the points, if path differences between points can be neglected. Although this simple method permits to combine several points from the acoustical standpoint, one should be aware that slight modifications of the electrical field lines are likely to change deeply the discharge regime, and thus the source terms. A first experimental study of this phenomenon[32] shows that the values of the $\mathcal{K}(V_i - V_a)$ and $\beta = I_e/I_i$ factors are very different for a repartition of multiple points close one to the other, compared to the values for a single point.

III. EXPERIMENTAL ANALYSIS OF DIFFERENT CONFIGURATIONS

This section is devoted to an analysis of the influence of the most significant parameters of a plasma loudspeaker. It is based on experimental investigations of a single point unit, which requires a dedicated set-up because of the low acoustic pressures involved.

A. Experimental set-up

Most of the experimental set-up used here is described in detail in a previous paper[33], so only specific parts are recalled below (when necessary to interpret response data collected from experimental set-up). Experiments have been conducted using very simple configurations of the electrodes, in order to be close enough to the model assumptions used in the previous part. The electrode system is made up of a stainless steel needle connected with a $1 M\Omega$ resistance (see Figure 4). The needle axis is placed perpendicular to a circular flat steel wire gauze (mesh $0.05 \times 0.05\ mm^2$; $\emptyset_{wire} = 0.03\ mm$), assumed to be acoustically transparent. Most of the measurements have been made using needles having different tip radii of curvature and materials. The needle (with series resistor) and the gauze are held by a thin plastic frame, designed to have little effect on the acoustic field. This frame allows the needle-to-grid gap to be varied from 3 to 10 mm.

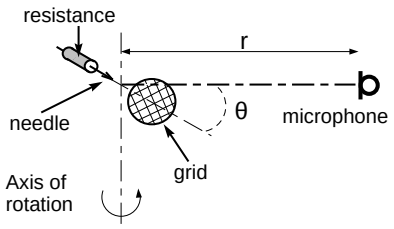

FIG. 4. Electrodes of the experimental needle-to-grid system.

The supply voltage values V_{HT} are in the range 3 to $10\,kV$ with a resulting DC current value I in the range of 30 to $100\,\mu A$. The voltage modulation is about $10\,V_{rms}$ which leads to a modulation degree lower than 0.5 %. This little value limits the acoustic field radiated by the system, but avoids any non-linearity of the loudspeaker. All the measurements are carried out in the "pulseless" regime, so that the pulse frequency is far greater than the audio frequencies, and the pulsed part of the current is small (ripple lower than 10 %).

Two microphones are used to measure the acoustic pressure generated by the discharge : a Brüel and Kjaer 1/4 inch condenser microphone for measuring frequencies up to $10\,kHz$, and an 1/8 inch condenser microphone for higher frequencies. The 1/8 inch microphone could not be used over the total frequency range because of its noise level, whereas the 1/4 inch microphone induced too much diffraction at higher frequencies. Considering the low pressure levels measured ($0 - 60\,dB_{SPL}$), the electrical signals issued by the microphone cartridge are amplified and filtered respectively by a microphone

amplifier and a 1/3 octave filter. Furthermore, an electromagnetic shield, assumed to be transparent to the acoustic waves, is used to protect the microphones against the non-negligible electromagnetic radiation from the transducer.

The scanned frequency range is limited to $[100\,Hz - 100\,kHz]$ by the available equipment. In the frequency range $[5\,kHz - 50\,kHz]$, the pressure signal has been measured at least $20\,dB$ above the essentially coherent background noise due to parasitic electromagnetic couplings. The voltages v_i and v_μ, respectively proportional to the AC current flowing through the air gap and the acoustic pressure, are measured using a lock-in amplifier (Stanford Research SR850) via a self-made multiplexer, so the transfer function (v_μ/v_i) can be composed. The demodulation parameters are optimised carefully to allow an accurate signal measurement in a relatively short time, avoiding in this way the alteration of experimental conditions with time.

B. Frequency response and directivity

Figure 5 shows an example of the measured directivity curves and the on-axis acoustic pressure. This directivity curve, like the ones obtained for other experimental conditions, displays a directivity pattern very close to a supercardioïd, resulting from the sum of a monopole and a dipole.

The frequency response and the directivity curve give a global acoustic pressure response of the plasma loudspeaker. Our approach makes use of the models described above (Eqs. 2 and 4), in order to separate the responses associated with each acoustic source. This approach starts with the measured acoustic pressure which can be modelled as follows[32,33,50] :

$$\begin{aligned} p(r,\omega) &= p_m(r,\omega) + p_d(r,\omega) \\ &= (A + B\cos\theta)\frac{e^{-jkr}}{r} i(\omega) \end{aligned} \tag{5}$$

where p_m and p_d have a directivity with respectively a monopolar and a dipolar character.

By plotting the amplitude of $p(r,\omega)$ versus $cos(\theta)$, and using a linear regression, factors A and B can be deduced from the directivity curve at each frequency. Validity of this method is checked by plotting the difference between the modelled pressure and the measured one, which usually varies almost randomly with respect to the angle θ. The adjusted pressures p_m and p_d are then respectively associated to the theoretical pressures p_h and p_f (Eqs. 2 and 4), allowing us to estimate the two adjustable parameters $\mathcal{K}(V_i - V_a)$ and $\beta = I_e/I_i$ from the pressure levels generated by both source terms. Figure 5 displays a comparison between the measured acoustic pressure of a needle-to-grid system, and the one deduced from the models, with parameters $\mathcal{K}(V_i - V_a)$ and $\beta = I_e/I_i$ adjusted for best fit with experimental data.

In the frequency range considered, the measured frequency response shows a straight line with a slope of $+6\,dB/octave$ from about 3 to $15\,kHz$. At lower frequencies, the pressure is too low to get a good estimate all around the needle-to-grid, but the behaviour of the transducer is likely to follow smoothly a simple asymptotic behaviour. At higher frequencies, diffraction occurs on various components of the measuring system. Diffraction on the microphone body has not been compensated, which may explain the discrepancies for frequencies higher than $30\,kHz$, for which the model also predicts a cut-off of the force source as the electrodes spacing is close to half a wavelength.

The agreement between the models and the measurements may so be considered as satisfactory up to $20\,kHz$. This measurement setup therefore provides a mean for estimating the acoustic pressures associated with the heat and the force sources in most of the audio frequency range. Consequently, it allows to observe variations of the response of each acoustic source when changing the electric and geometric configurations of the plasma loudspeaker.

C. Influence of the electric and geometric configurations

The discharge current I, the electrode separation d, and the tip radius ρ_c are parameters which may change the spatial repartition of the electric field inside a discharge and consequently these parameters influence the discharge regime, the acoustic behaviour, and finally the electroacoustic efficiency of the plasma loudspeaker. Figures 6 and 7 show the acoustic pressure versus the DC current I and the gap length d respectively, estimated for each source (heat and force) at $r = 10\,cm$ from the gap centre of a needle-to-grid system (with $d = 3\,mm$, $\rho_c = 20\,\mu m$, $f = 5\,kHz$). In this geometric and electric configuration, the sound level due to the force source is observed to be about $6\,dB$ greater than the level due to the heat source in the frequency range $(2 - 20\,kHz)$[32,33,50].

In figures 6 and 7, the two parameters β and $\mathcal{K}(V_i - V_a)$ of the theoretical results p_h, p_f (eqs. 2 and 4) are adjusted to fit the first experimental result for p_m, p_d (eq. 5), and kept constant when varying d or I. This leads to an increasing discrepancy between the predictions p_f

and experimental results p_d as DC current I increases (figure 6). In the same manner, discrepancies between the predictions p_h, p_f and experimental results p_m, p_d become more and more important as the gap length d increases (figure 7). These observations clearly indicate that the two unknown parameters are dependant on d and I, albeit there is almost no litterature about this topic.

Many experimental values for the adjustable parameters have been obtained by Castor[50], and only the main tendancies observed during these experiments are summarised hereafter. The parameter $\mathcal{K}(V_i - V_a)$ was found to increase with the gap length d or DC current I. Furthermore, with a needle using a brass or a stainless material (respectively a copper or a steel material), this parameter decreases (respectively increases) with increasing radius of curvature ρ_c. β is deduced to have a value around 2, with its value increasing with DC current I and almost independent of the distance d. With a needle using a brass or a stainless material (respectively a copper or a steel material), the parameter β was found to increase (respectively decrease) with increasing radius of curvature ρ_c. Finally, it is interesting to note that smaller is the gap length d, the greater is the dependence between the two parameters (β, $\mathcal{K}(V_i - V_a)$) and the radius of curvature ρ_c.

IV. POWER EFFICIENCIES

In order to design and optimise a plasma loudspeaker, it is important to model the evolution of the electroacoustic efficiency of each source with the geometric and electric configurations. To our knowledge, no investigation has been yet carried out in this direction, apart from some earlier work without electric modulation : owing to the complexity of the energy exchanges between charged and neutral particles, the fraction of the electric energy transformed into thermal form and kinetic form (wind) has been roughly estimated to be around $20\,\%$[7,8,10] and $5\,\%$[5,51] respectively. This section thus describes measurements of dynamic input (electric) and output (acoustic) powers involved in the plasma loudspeaker.

A. Electric power

The dynamic part of the electric power associated with the needle-to-grid system can be expressed as[50,52] :

$$P_e = \frac{1}{2}\Re e[v(\omega).i^*(\omega)] = \Re e[Z(\omega)].|i(\omega)|^2 \qquad (6)$$

where v, i and Z are the AC voltage between the electrodes, the AC current flowing through the electrodes, and the electrical impedance. The asterisk denotes complex conjugation.

This electrical power can be divided in two parts. One is associated with the ionisation region :

$$P_{ei} = r_i \cdot |i_{RMS}(\omega)|^2 \qquad (7)$$

and other one is associated with the drift region :

$$P_{ed} = \frac{r_u}{1 + (\omega r_u C_u)^2} \cdot |i_{RMS}(\omega)|^2 \qquad (8)$$

From these expressions is deduced that the total electrical power is constant at low frequency and equal to :

$$P_{et} \approx (r_i + r_u) \cdot |i_{RMS}(\omega)|^2 \qquad (9)$$

This evolution is observed on figure 8, in which the measured electrical power is around a few microWatts, and relatively constant with frequency up to $20\,kHz$. Its value then increases slightly at higher frequencies. A similar frequency behaviour of the electrical power is observed whatever the geometrical and the electrical configurations of plasma loudspeakers[32].

B. Acoustic power

The intensity vector $\mathbf{I}$, which describes the energy flow in an acoustic field, is defined as the time average of the product of acoustic pressure p and particle velocity $\mathbf{v}$. Integrated over an area S, the intensity gives the acoustic power flow through this area. In the present case, the plasma loudspeaker is considered as the centre of a sphere of radius r, which surface S thus totally encloses the acoustic sources. Assuming a far-field condition, the pressure and the velocity are related by the characteristic impedance of air, and intensity is a function of the pressure which can be integrated over the sphere to get the radiated acoustic power.

As the electrical power, the acoustic power is divided in two parts. On the one hand we assume that the acoustic power delivered by the heat source corresponds to the monopolar component of the pressure response, and on the other hand that the dipolar component must be associated with the force source term. The acoustic power expressions associated with the ionisation region and the drift region are then respectively[50,52] :

$$P_{ah} \approx \frac{1}{4\pi}\,\frac{1}{\rho_0 c_0}\,\left(\frac{\omega}{c_0}\right)^2\,\left(\frac{\gamma - 1}{c_0}\right)^2 \cdot [\mathcal{K}(V_i - V_a)]^2\,|i_{RMS}(\omega)|^2 \qquad (10)$$

and

$$P_{af} \approx \frac{1}{12\pi}\,\frac{1}{\rho_0 c_0}\,\left(\frac{\omega}{c_0}\right)^2\,\left(\frac{d}{\mu_i(\beta+1)}\right)^2 \cdot \frac{1}{1+(\omega r_u C_u)^2}\,|i_{RMS}(\omega)|^2 \qquad (11)$$

Both these relations show a dependence on the frequency, the geometric and the electric configurations of the plasma loudspeaker. An experimental work of Castor[50] on needle-to-grid plasma loudspeaker reveals that the measured acoustic power associated with each source are very low; the values estimated are around a few picoWatts, these very low values resulting in a great part from the low electric modulation degree ($v_{modulation}/V_{HT} \ll 1$) required by the experimental set-up.

C. Efficiencies

The electroacoustic efficiency η_h (respectively η_f) associated with the heat source (respectively the force source) is the ratio of the time-averaged acoustic power P_{ah} (respectively P_{af}) to the time-averaged electric power P_{ei} (respectively P_{ed}) :

$$\eta_h = \frac{P_{ah}}{P_{ei}} = \frac{1}{4\pi}\frac{1}{\rho_0 c_0}\,\left(\frac{\omega}{c_0}\right)^2\,\left(\frac{\gamma-1}{c_0}\right)^2\,\frac{[\mathcal{K}(V_i-V_a)]^2}{r_i} \qquad (12)$$

$$\eta_f = \frac{P_{af}}{P_{ed}} \approx \frac{1}{12\pi}\frac{1}{\rho_0 c_0}\,\left(\frac{\omega}{c_0}\right)^2\,\left[\frac{d}{\mu_i\,(\beta+1)}\right]^2\,\frac{1}{r_u} \qquad (13)$$

Both electroacoustic efficiencies increase with the square of the frequency ($+12\,dB/octave$). They also depend on many parameters, associated with the weakly ionised air (γ ,ρ ,c_0 and μ_i), the electric configuration (r_i, r_u, $\mathcal{K}(V_i-V_a)$ and β) and the gap length d. However all the electrical parameters are themselves dependant on the geometric configuration of the electrodes, so the actual number of parameters is in fact much lower than in the above expressions. For a given needle (material and radius of curvature ρ_c), the effective "tunable" parameters are thus only I and d.

D. Measurements and tendancies

Experimental estimations of efficiencies are presented in figure 9, showing the practical importance of the main parameters defining the needle and the configuration. The two efficiencies for each source term are first presented separately, after an identification of the monopole and dipole radiated fields, and then the efficiency of the transducer is studied as whole. Comparison of these curves allows to discuss the influence of parameters, and to propose an optimum configuration.

The electric current crossing the ionisation and the drift region being the same, the electric power (associated to the electric modulation) is principally transferred to drift region which has the higher electric impedance (eq. 8). While the electric power transferred to the heat source is relatively low (eq. 7), its estimated contribution to the total acoustic power (eq. 10) is generally 25 % higher than the force source contribution (eq. 11).

Consequently, the efficiency associated with the heat source η_h is generally about twenty times higher than the one associated with the source force η_f (fig. 9 a,b). However, even with such a higher efficiency of the heat source, the global energetic behaviour of the transducer is observed to be governed mainly by the drift region, which absorbs most of the modulation input power (fig. 9 c).

Whatever the value of the electric current I in the range 20 to 100 μA, the total electroacoustic efficiency (following the one associated with the source force) increases with increasing gap length (d = 6 and 8 mm). This behaviour depends on the needle material : with needle using titanium, steel or brass material a roughly linear relation is observed between efficiency and gap length, whereas for stainless needle this linear relation disappears.

With a needle using a brass or a stainless material (respectively a copper or a steel material), the total electroacoustic efficiency decreases (respectively increases) with increasing radius of curvature (ρ_c = 50 μm and 100 μm).

Due to the previous considerations, and in order to obtain a needle-to-grid plasma loudspeaker with an optimal efficiency, a system using a steel or a stainless needle with a small radius curvature placed at 1 cm from the grid and fed with a DC current in the range of 70 to 90$\mu\,A$ would be recommended. Note that with a greater gap length or DC current, electric instabilities appear in the discharges, leading to undesirable random acoustic emission.

V. CONCLUSION

The electrode gap in negative needle-to-grid corona discharge loudspeaker is divided into an ionisation region

near the point and a drift region. In each region, interactions between charged and neutral particles in the ionised gas lead to a perturbation of surrounding air and so generate an acoustic field. For each region, seen as an independent acoustic source, a specific acoustical model is developed with monopolar and dipolar characters associated with the ionisation and drift region respectively. Their major limitation is that both need to adjust a parameter related to electrical configuration. A work on the electrical, the acoustic power, and the electroacoustic efficiency of the loudspeaker has been realised. The main properties which result from this work are the following :

1. The plasma loudspeaker has directivity curves that are close to a supercardioid pattern, almost constant over the audio frequency range.
2. The amplitude of the pressure acoustic associated with the source force (drift region) with dipolar behaviour is measured with approximately twice the amplitude of the pressure acoustic associated with the heat source (ionisation region) with monopolar behaviour.
3. The gross physical properties of the plasma loudspeaker which determine the amplitudes of the acoustic pressures associated with each source are the needle material and radius of curvature, and the distance between the two electrodes. The DC current feeding the discharge may be adjusted in a small range for a given electrode configuration.
4. Although both sources have a similar importance in terms of radiated pressure, the heat source has a much greater efficiency - but the total efficiency is still governed by the force source term.

These conclusions are still preliminary, as the range of possible materials, tip geometries and electrode configurations is obviously much wider than the one covered in the present work. Our results seem however in accordance with most of the ones published until now - concerning negative DC Corona discharges.

According to the theoretical investigations of plasma loudspeaker proposed in this paper, the acoustic pressure generated by this system is directly proportional to the modulation of the electric current flowing between the electrodes. When an oscillating electric field is provided by voltage modulation of the needle-to-grid system, due to the non linear current-voltage $I - V_{HT}$ characteristic (see Figure 2), current harmonic distortion and consequently acoustic pressure distortion are however expected. In the previous section, this non linear behaviour is minimised by using a low voltage modulation degree ($v_{modulation}/V_{HT} < 0.5\,\%$), but the acoustic power generated by the needle-to-grid system is then very limited. The following topics are thus considered to merit further study, in order to assess the actual performances of a future unit :

1. In order to obtain higher acoustic pressure level and avoid the effect of the non linear current-voltage ($I - V_{HT}$) characteristic on the pressure frequency response, a current modulation should be used, allowing a higher modulation degree.
2. A modelling and an analysis of non linearities of the acoustics sources (heat and force) should then be developed, and compared to experimental studies of the distortion in the plasma loudspeaker.
3. Theoretic and experimental studies of the plasma loudspeaker with other geometric configurations (*e.g.* wire-to-plane system) and multiple electrode systems could also be envisaged, provided that a suitable model of its electric behaviour can be proposed.

VI. ACKNOWLEDGEMENTS

The authors would like to thank Guy Tournois and Alain Brunet for their assistance in the experiments and their technical advices.

[1] F. Bastien, "Acoustic and gas discharges : applications to loudspeakers", J. Phys. D : Appl. Phys. **20**, 1547–1557 (1987).

[2] M. S. Mazzola and G. M. Molen, "Modeling of a dc glow plasma loudspeaker", J. Acoust. Soc. Am. **81**, 1972–1978 (1987).

[3] H. Bondar, "Haut-parleur vers une ère nouvelle", Nouv. Rev. **58**, 71–79 (1982).

[4] H. Bondar, "Un haut-parleur à plasma froid", Nouv. Rev. **59**, 73–80 (1982).

[5] A. Deraedt, "electroacoustic transducer using corona effect", in *Proc. 90^{th} Audio Engineering Society Convention*, volume preprint 3037, 1–19 (A.E.S., Paris, France) (1991).

[6] M. Fitaire and T. Mantei, "Some experimental results on acoustic wave propagation in plasma", Phys. Fluids **15**, 464–469 (1972).

[7] P. Bayle, M. Bayle, and G. Forn, "Neutral heating in glow to spark transition in air and nitrogen", J. Phys. D : Appl. Phys. **18**, 2395–2415 (1985).

[8] P. Bayle, M. Bayle, and G. Forn, "Blast wave propagation in glow to spark transition in air", J. Phys. D : Appl. Phys. **18**, 2417–2432 (1985).

[9] P. M. Morse and K. U. Ingard, *Theoretical Acoustics, Ch 12 : Plasma acoustics* (Princeton University Press, Princeton, New Jersey) (1986).

[10] O. Eichwald, M. Jugroot, P. Bayle, and M. Yousfi, "Modelling neutral dynamics in pulsed helium short-gap spark discharges", J. Appl. Phys. **80**, 694–709 (1996).

[11] M. Goldman and A. Goldman, *Gaseous electronics, Ch.4 : Corona discharges*, volume 1 (Academic Press, New York) (1978).

[12] E. E. Kunhardt and L. H. Luessen, *Electrical breakdown and discharges in Gases* (Plenum Press, New York) (1982).

[13] E. Nasser, *Fundamentals of Gaseous ionisation and plasmas electronics*, volume 1 (Wiley, New york) (1971).

[14] Y. P. Raiser, *Gas discharge physics* (Springer-Verlag, Berlin Heidelberg) (1991).

[15] W. L. Lama and C. F. Gallo, "Systematic study of the electrical characteristics of the trichel current pulses from negative needle-to-plane coronas", J. Appl. Phys. **45**, 103–113 (1974).

[16] R. S. Sigmond, "Simple approximate treatment of unipolar space-charge-dominated coronas : The warburg law and the saturation current", J. Appl. Phys. **53**, 891–898 (1982).

[17] R. S. Sigmond, "The residual streamer channel : return strokes and secondary streamers", J. Appl. Phys. **56**, 1355–1370 (1984).

[18] G. F. L. Ferreira, O. N. Oliveira, and J. A. Giacometti, "Point-to-plane corona : Current-voltage characteristics for positive and negative polarity with evidence of an electronic component", J. Appl. Phys. **59**, 3045–3049 (1986).

[19] W. R. Babcock, K. L. Baker, and A. G. Cattaneo, "Music flames", Nature **216**, 676–678 (1967).

[20] M. Fitaire and D. Sinitean, "Excitation d'ondes acoustiques par une flamme", Czech. J. Phys. **B**, 394–397 (1972).

[21] M. S. Sodha, V. K. Tripathe, and J. K. Sharma, "flame loudspeakers", Acustica **40**, 68–69 (1978).

[22] P. Riety, "Retour sur la théorie du thermophone à feuilles d'or", Cahiers d'Acoustique **70**, 169–201 (1955).

[23] F. J. Fransson and E. V. Jansson, "The stl-ionophone : transducer properties and construction", J. Acoust. Soc. Am. **58**, 910–915 (1975).

[24] L. D. Lafleur, J. J. Matesse, and R. L. Spross, "Acoustic refraction by a spark discharge in air", J. Acoust. Soc. Am. **81**, 606–610 (1987).

[25] M. Akram and E. Lundgren, "The evolution of spark discharges in gases : Macroscopic models", J. Phys. D :Appl. Phys. **29**, 2129–2136 (1996).

[26] S. Klein, "L'ionophone", Onde Electr. **26**, 314–320 (1946).

[27] S. Klein, "Cellule thermionique de grande puissance a atmosphère gazeuse et ions positifs", Onde Electr. **26**, 367–373 (1946).

[28] S. Klein, "French patent specification 79 09450", (1979).

[29] K. Matsuzawa, "Sound sources with corona discharges", J. Acoust. Soc. Am. **54**, 494–498 (1972).

[30] P. Béquin, "Modèles de sources acoustiques à gaz ionisé", Ph.D. thesis, Université du Maine, Le Mans, France (1994).

[31] P. Béquin and P. Herzog, "Model of acoustic sources related to negative point-to-plane discharges in ambiant air", Acta Acustica **83**, 359–366 (1997).

[32] V. Montembault, "Etude des sources acoustiques associées aux décharges corona négatives", Ph.D. thesis, Université du Maine, Le Mans, France (1997).

[33] P. Béquin, V. Montembault, and P. Herzog, "Modelling of negative point-to-plane corona loudspeaker", Eur. Phys. J. AP **15**, 57–67 (2001).

[34] D. M. Tombs, Nature **176**, 923 (1955).

[35] G. Shirley, "The corona wind loudspeaker", J. Audio Eng. Soc. **5**, 29–37 (1957).

[36] M. Boutlendj and N. L. Allen, "Current-density distribution on a plane cathode in dc glow and streamer corona regime in air", IEEE Trans. Electr. Ins. **28**, 86–92 (1993).

[37] Y. S. Akishev, I. V. Kochetov, A. P. Napartovich, and N. I. Trushkin, "The generation-zone structure in negative corona discharges", Plasma Phys. Rep. **21**, 179–183 (1995).

[38] A. P. Napartovich, Y. S. Akishev, A. A. Deryugin, I. V. Kochetovand M. V. Pan'kin, and N. I. Trushkin, "A numerical simulation of trichel-pulse formation in a negative corona", J. Phys. D : Appl. Phys. **30**, 2726–2736 (1997).

[39] Y. S. Akishev, M. E. Grushin, I. V. Kochetov, A. P. Napartovich, and N. I. Trushkin, "Establishment of regular trichel pulses in a negative corona in air", Plasma Phys. Rep. **25**, 922–927 (1999).

[40] A. E. Seaver, "An engineering equation for corona devices", IEEE Industry Applications Magazine 30–35 (1995).

[41] R. Morrow, "Theory of negative corona in oxygen", Phys. Rev. A **32**, 1799–1808 (1986).

[42] M. Robinson, "Movement of air in the electric wind of the corona discharge", Trans. Am. Inst. Elect. Engin. **80**, 143–152 (1961).

[43] L. C. Thanh, "Similitude between ionic wind discharge pattern and corona current", Electron. Lett. **15**, 57–58 (1979).

[44] R. S. Sigmond, "Mass transfer in corona discharges", Rev. Int. Hautes Tempér. Réfract. **25**, 201–206 (1989).

[45] R. S. Sigmond, A. Goldman, and M. Goldman, "Ring vortex gas flow in negative point coronas", in *Proc. 10^{th} Int. Conf. On Gas Disch. And their Appl.*, 330–333 (Swansea, U.K.) (1992).

[46] R. S. Sigmond and I. H. Lâgstad, "Mass and species transport in corona discharges", Plasma Phys. Rep. **2**, 221–229 (1993).

[47] J. Batina, F. Noël, S. Lachaud, R. Peyrous, and J. F. Loiseau, "Hydrodynamical simulation of the electric wind in a cylindrical vessel with positive point-to-plane device", J. Phys. D : Appl. Phys. **34**, 1510–1524 (2001).

[48] P. Béquin, K. Castor, and J. Scholten, "Electric wind characterisation in negative point-to-plane corona discharges in air", Eur. Phys. J. AP. **22**, 41–49 (2003).

[49] M. M. Kekez, P. Savic, and G. D. Lougheed, "A novel treatment of trichel type phenomena with possible application to stepped-leader phenomena", J. Phys. D : Appl. Phys. **15**, 1963–1973 (1982).

[50] K. Castor, "Caractérisation des sources acoustiques associées aux décharges couronnes négatives", Ph.D. thesis, Université du Maine, Le Mans, France (2001).

[51] H. Bondar and F. Bastien, "Effect of neutral fluid velocity on direct conversion from electrical to fluid kinetic energy in an electro-fluid-dynamics (efd) device", J. Phys. D : Appl. Phys. **19**, 1657–1663 (1986).

[52] K. Castor and P. Béquin, "Rendement d'un haut-parleur à décharges corona négatives", in *Proc. 5^{th} Int. French Congress On Acoustics*, 676–679 (Lausanne) (2000).

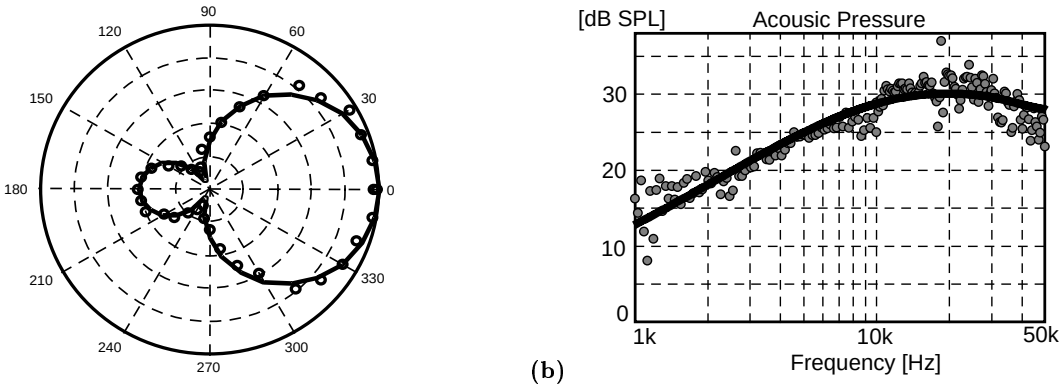

FIG. 5. **(a)** Directivity curve ($f = 5\,kHz$), the acoustic pressure is normalised with respect to the on-axis ($\theta = 0$) value. **(b)** On-axis acoustic pressure versus frequency. (ooo) experimental results ; (——) theoretical predictions (Eqs. 2 and 4). Configuration of the needle-to-grid system : $d = 6\,mm$, $I = 60\,\mu A$, $i = 0.3\,\mu A$, $r = 10\,cm$.

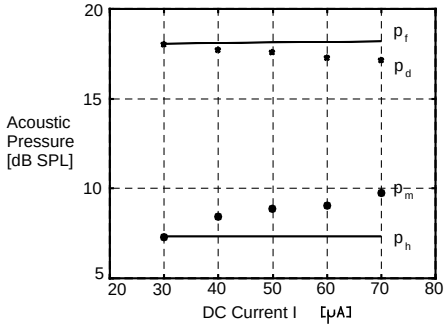

FIG. 6. Sound pressure level measured on the axis of the needle-to-grid systems at $r = 10\,cm$ ($d = 3\,mm$, $\rho_c = 20\,\mu m$, $i_{mean} = 0.38\,\mu A$, and $f = 5\,kHz$). ($\star$,o) Experimental results associated with p_d and p_m ; (—) theoretical predictions associated with p_h and p_f in which the adjusted parameters are $\beta \approx 1.9$ and $\mathcal{K}(V_i - V_a) \approx 1.4\,kV$.

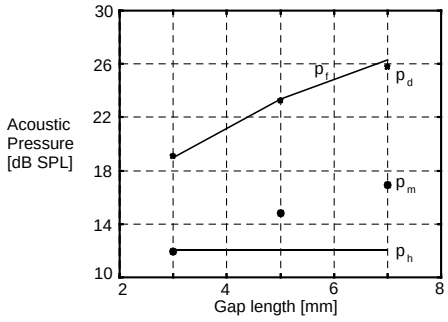

FIG. 7. Sound pressure level measured on the axis of the needle-to-grid systems at $r = 10\,cm$ ($\rho_c = 20\,\mu m$, $I = 70\,\mu A$, $i_{mean} = 0.53\,\mu A$, and $f = 5\,kHz$). ($\star$,o) Experimental results associated with p_d and p_m ; (—) theoretical predictions associated with p_f and p_h, in which the adjusted parameters are $\beta \approx 2.6$ and $\mathcal{K}(V_i - V_a) \approx 1.8\,kV$.

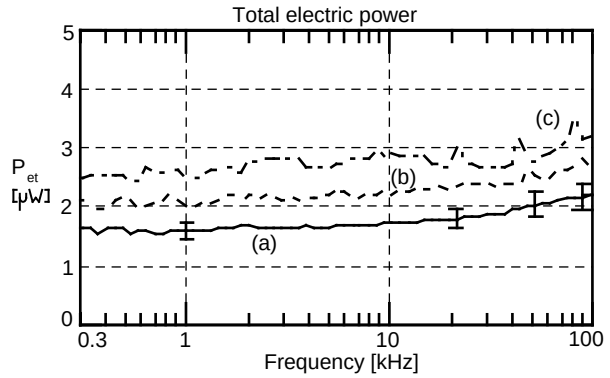

FIG. 8. Electrical power measured on the plasma loudspeaker with the geometrical configuration $d = 3\,mm$, and $\rho_c = 20\,\mu m$, and with three electric configurations (a) $I = 30\,\mu A$, $V = 4\,kV$; (b) $I = 50\,\mu A$, $V = 4.6\,kV$; (c) $I = 70\,\mu A$, $V = 5\,kV$.

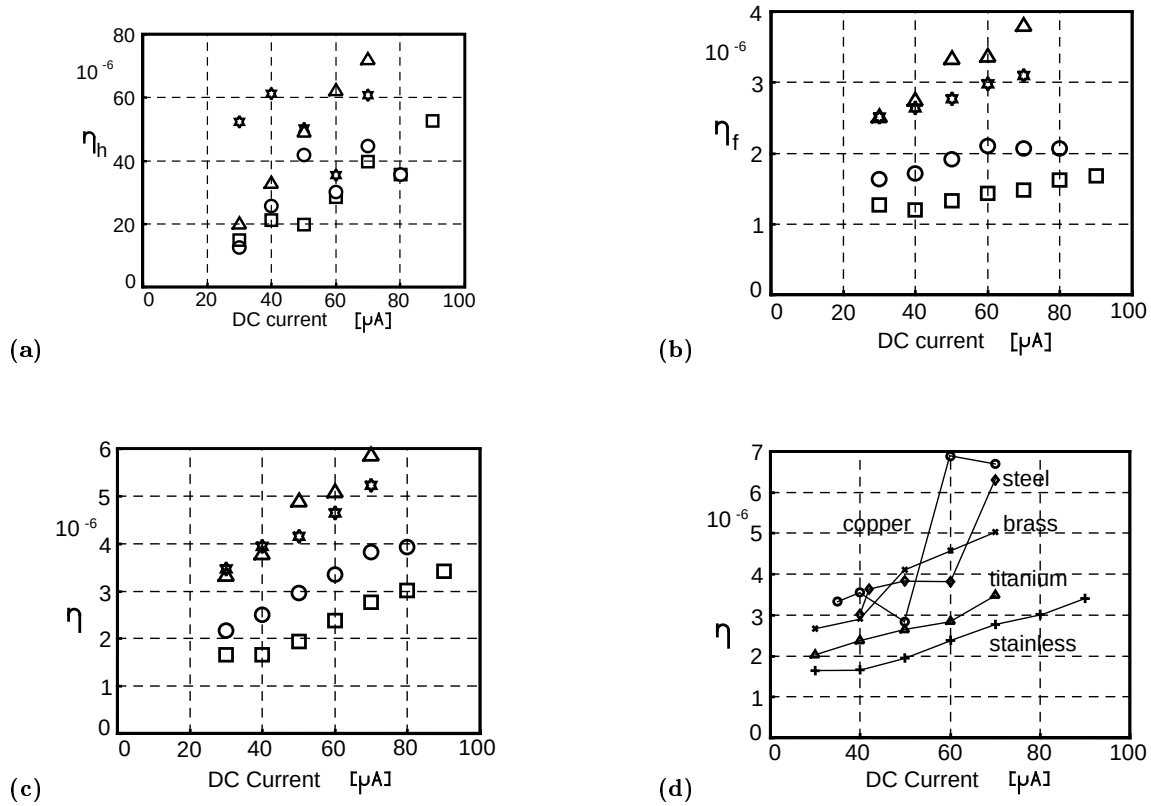

FIG. 9. Electroacoustic efficiency associated with **(a)** the heat source , **(b)** the force source. **(c)** and **(d)** the total electroacoustic efficiency [50,52].(□,o) d=6mm ; (★,△) d=8mm and (△,o)$\rho_c = 50\mu m$; (□,★) $\rho_c = 100\mu m$.